Interactive comment on "Thickness of the lithosphere beneath Turkey and surroundings from S-receiver functions" *by* R. Kind et al.

W.H. Geissler (Referee)

wolfram.geissler@awi.de Received and published: 3 May 2015

RESPONSES and corrections are marked in red

Dear authors,

your submission is a highly valuable contribution to better understand the lithosphere, its deep structure and processes related to plate tectonics, not only in the regional context of the Anatolian subplate. I really like your work and most of the way it is presented. I only have some minor comments, which may help to further improve the publication and its impact.

First of all I would ask you to restructure your manuscript in a way that the observation/results are more separated from your interpretation and discussion. You tried to do this, but in my opinion it is still not clear enough. We have structured our paper by geological units like LAB or Slab. Each section contains an observational and an interpretational part. Of course, it could be organized in different ways, which serve all more or less the same purpose.

To show the general structure you decided to apply a low pass filter with a corner period of 8 s. As you also stated that might prevent to observe more regional and local features such as the extent of fault zones. I would suggest to further exploit cross sections with filters of different corner periods (see figure 11b and c). Figure 11 shows that the LAB is a very different discontinuity compared, for example, with the Moho or the 410 and 660 discontinuities. If we use shorter periods, the Moho and 410 and 660 get sharper, whereas the LAB dissolves in in a number of laminated discontinuities. We have added to our other discussion paper on the USArray in the same special volume (Kind et al. (2015)) figures showing the same observation even more clearly in North America. If we could drill a hole to the apparently exactly measured location of the longperiod observation of the LAB, we might find nothing because the longperiod LAB is only the mean over a larger horizontal and vertical region. Study of the small scale lamellae would need a much larger observational effort. We have pointed out these problems in more detail in the paper. It is an important and not widely known result that the character of the discontinuities in the mantle lithosphere (LAB and also MLD in North America) is very special and that its depth and also the amplitude of the converted signals depend on the periods used for the observation. Our goal was to show the general large scale structure. For this the 8s filter seems perfect. Shorter period filters would require much denser data to obtain reliable results. Earlier long range controlled source profiles in western Europe (for example Kind 1974) found such a laminated structure in the mantle lithosphere.

On page 1325, in my opinion, you mix the slab break-off scenarios with lithosphere evolution of Anatolia. This paragraph needs some clarification. Slab belongs to the African plate, the lithosphere to the Anatolian subplate. Thanks for pointing this out. We have moved the part on the general Anatolian LAB to Section 5.2.

On page 1326, you mix the naming of the slabs (or use different names for the same structures). Please make this more coherent. Why the Aegean Slab is not called Hellenic. That would make more sense to name it like the Arcs. We have done so.

Page 1327, You discuss that the NAF is not linked to a deep deformation zone, but your only indication is the anisotropy pattern (could you plot this pattern on one of the maps)? How the NAF should work if it would not be a deep-reaching fault zone? Unfortunately, your data in the presented resolution provides no new insights into the topic. What are with anomalies (converters) imaged below the assumed LAB? Some of them seem to mimic the tectonic provinces at the surface (figures 5 to 10, especially 9). Our mentioning of the anisotropy is only a reference to other papers. We do not have own anisotropy data. We make this more clear in the text. Our result is that the structure down to the LAB is similar on both sides of the fault. We cannot conclude from this that the NAF is not deep reaching. Our results merely indicate that the lithospheric thickness on both sides of the fault is very similar. We think signals from below the LAB are too weak to be interpreted.

Page 1328, where in your data you see the 150 km thick lithosphere? This is a reference to Sodoudi et al. (2006) for lithosphere in the northern Aegean.

The quality of figures is very good! In figure 6 you did not mark the 410? Figure 8: How it looks in 3D, if the Hellenic slab dips below the Cyprus slab? On some plots the marked LAB does not seem to follow the centre of the blue anomaly. We have marked the 410 also in Fig.6. We think our resolution is not yet good enough for a 3D image of the Hellenic and Cyprus slab. We have moved the smoothed LAB marks more to the center of the signals.

I would suggest to add a figure showing the depth to LAB in a map view accompanied by a table with coordinates and depth values. We think exact numbers on LAB depths derived from the 8 sec filtered data would be misleading since, as for example unfiltered data in Fig.11A show, the LAB consists of several small scale discontinuities. Mapping these discontinuities requires much higher effort. With 8 sec data we can only get a first order approximation of the LAB depth (80-100 km below Anatolia) which we would hesitate to map.

Interactive comment on "Thickness of the lithosphere beneath Turkey and surroundings from S-receiver functions" *by* R. Kind et al.

Anonymous Referee #2

Received and published: 8 May 2015

General Comments:

This is an interesting paper presenting a substantial Sp receiver function data set for Turkey,

aimed primarily at constraining the LAB in the region. The methods used are well-established and sound, and appear to have been applied with care (e.g. using synthetics to test the CCP image's ability to recover dipping features). I do think that there are aspects of the processing that could be a bit better explained, and that some aspects of the interpretation go a bit far given what is visible in the seismic images. I recommend publication after a minor revision to attend to the specific points noted below.

Specific comments:

* In terms of methodology: the deconvolution approach used and the type of filters applied should be explained in a sentence or two. I mention this in particular because Figure 3 shows strong negative sidelobes on both sides of the SPn arrival. Are those a deconvolution/filtering artefact, or something related to that particular phase? If the deconvolution or filtering are introducing sidelobes, then the possibility that the lithospheric arrival is in fact a sidelobe of the Moho arrival needs to be ruled out. I don't think this is actually the case, but it should be checked. We have commented on that. Seismic signals are causal. That means there is no signal in the records before the arrival time. This is valid for unfiltered seismic records. We compared LAB signals of unfiltered and undeconvolved traces with filtered and deconvolved traces and found no significant difference. This proves that our LAB data are not sidelobes and that our filters used are not producing significant sidelobes.

* Some of the dashed lines on the CCP sections go beyond what the underlying seismic image seems to call for. In Fig. 5, the "Afr. Moho" and "Afr. LAB" lines are drawn with steeper dips than the data call for – the seismic image shows a break in the Moho and a deflection of the LAB, but I don't think a dip angle can really be measured here. The lines in Fig. 6 is also a stretch, given that the LAB looks fairly continuous in the CCP and time images. Given how spotty the LAB is in the CCP panel of Fig. 8, interpreting a break in it is a subjective exercise (though the time panel looks more convincing). We think the inclined African Moho and LAB are clear in Fig.5. However we did not measure the inclination angle. For this purpose a differently scaled figure would be necessary. If we compare Figs. 5 and 6, we think we can still justify the the observation of the African slab in Fig. 6, although it is not as clear any more as in Fig.5. We agree that in Fig.8 the time domain image is clearer than the depth domain image. For that reason it is a good idea to have both types of images.

* Several images are unnecessarily tiny, at least in my "printer friendly" copy. Fig. 4 is almost indecipherable, particularly panel (g), and should be rearranged to take best advantage of the wider-than-tall space available on the page. The map panels in Figs 5 through 10 are also a bit small, as are the panels in Fig. 11. We will make sure that in the final version the size of the figures will be increased.

* Fig. 9 shows considerable variation in the 410 depth. I agree that the 410 is not the main focus of the paper, but the ca. 50 km of topography should be addressed: do the authors think it is real, or an artifact of lateral velocity variations versus the fixed velocity structure used for imaging? If the latter, are there implications for the interpreted LAB depths? We have commented on that. We suggest that the reason are lateral velocity variations between the LAB and 410. Large temperature variations in east-west direction at 400 km depth below Anatolia are perhaps less likely. It cannot be velocity variations above the LAB because the LAB does not have the same

variations.

* Page 1321, lines 13-15: "Figure 4g shows the emergent angle of the Sp converted wave at the lower boundary of the slab relative to the slab normal for the corresponding inclination angles of the slab as a function of the back azimuth." – this sentence took a while for me to make sense of. Maybe rephrase in a clearer way? We have done so.

* A pedantic point: the CCP stacking used is referred to as "migration" in a few places. I don't insist on this, because terminologies differ, but I'm reluctant to call CCP stacking "migration", given that it doesn't correct dip angles or collapse diffractions. We have replaced "migration" by "depth transformation".

* Page 1322, latter half of the paragraph: why are the criteria for including arrivals in the CCP and time images different? In the time images we took all rays with piercing points at 100 km in a fixed box. In the migrated images we took all rays which penetrated this box at any depth.

* The LAB arrival seen in this paper is at a depth similar to the mid-lithospheric discontinuity seen in some continental studies. This might be worth explicitly ruling out as an explanation for the observations (though I think it's obviously an LAB and not an MLD). This is an important question. The LAB in younger and tectonically active regions looks identical to the MLD in cratonic regions. However, the MLD got this name because the cratonic LAB is expected at larger depths. The deep cratonic LAB is indeed observed (in addition to the shallower MLD), also with receiver functions in a growing number of cratonic regions. Because in younger regions we see only one negative discontinuity in the lithosphere below the Moho, it is interpreted as LAB in the classical lithosphere-asthenosphere model.

Technical comments:

* Fig. 1: the black line denoting the Hellenic and Cyprean arcs is hard to see against the dark grey background. We changed that

* A few grammar/wording corrections (given in uppercase): all have been corrected

- Page 1316, line 10: "We did not observe changes IN LAB DEPTH across..." line 17: "The lower boundary of the lithospheric PLATE is a very..."

- Page 1317, line 9: "...are considered TO BE the main driving processes" line 14: "...ARE currently the major driving FORCES..." line 19: "...except FOR localized thrust ridges..."

- Page 1319, line 9: "...the P receiver FUNCTION TECHNIQUE..." line 19: "...the essential part of S-receiver functions CONSISTS OF weakly converted..."

- Page 1320, line 12: "A positive conversion... and a a negative... ARE clearly visible." line 16: "...meaning that they CUT ACROSS all other phases..."

- Page 1321, line 4: "Based on AN available reference..." line 5: "...is used as THE input model." line 11: "...would yield identical information TO THAT obtained..."

- page 1322, line 11: "...and the WIDTH of the section..."

- page 1323, line 25: "P-receiver FUNCTIONS are more useful for this purpose."

- page 1324, line 10: "Our observations... CONFIRM earlier results."

- page 1326, line 11: "...result from the Eratosthenes SEAMOUNT beneath Cyprus..."

- page 1327, line 1: "...we also do not observe any SIGNIFICANT contrast in the delay times..." line 4: "...although the data quality WORSENS..." line 6: "...inferred from the SKS measurements RELATIVE to the actual orientation..."

- page 1328, line 10: "...would not have been imaged by S receiver functions, HOWEVER."

Thickness of the lithosphere beneath Turkey and surroundings from S-receiver functions

Rainer Kind (1,2), Tuna Eken (1), Frederik Tilmann (1,2), Forough Sodoudi (1), Tuncay Taymaz (3), Fatih Bulut (5), Xiaohui Yuan (1), Birsen Can (4) and Felix Schneider (1)

(1) Deutsches GeoForschungsZentrum GFZ, Potsdam, Germany, (kind@gfz-potsdam.de)
(2) Freie Universität, Berlin, Germany
(3) Department of Geophysical Engineering, The Faculty of Mines, Istanbul Technical University, 34469 Maslak, Istanbul, Turkey
(4) Bogazici University, Kandilli Observatory and Earthquake Research Institute (KOERI), Istanbul, Turkey
(5) Istanbul Aydın University, AFAM D. A. E. Research Centre, Istanbul, Turkey

Abstract

We analyze S-receiver functions to investigate variations of lithospheric thickness below the entire region of Turkey and surrounding areas. The teleseismic data used here have been compiled combining all permanent seismic stations which are open to public access. We obtained almost 12,000 S-receiver function traces characterizing the seismic discontinuities between the Moho and the discontinuity at 410 km depth. Common-conversion-points stacks yield well-constrained images of the Moho and of the lithosphere-asthenosphere boundary (LAB). Results from previous studies suggesting shallow LAB depths between 80 and 100 km are confirmed in the entire region outside the subduction zones. We did not observe changes in LAB depths across the North and East Anatolian Faults. To the east of Cyprus, we see indications of the Arabian LAB. The African plate is observed down to about 150 km depth subducting to the north and east between the Aegean and Cyprus with a tear at Cyprus. We also observed the discontinuity at 410 km depth and a negative discontinuity above the 410, which might indicate a zone of partial melt above this discontinuity.

1 Introduction

The lower boundary of the lithospheric plate is a very important parameter for understanding plate tectonics, although it is still one of the less known quantities. Our current knowledge of the lithospheric thickness beneath Turkey relies on studies that examined the data from several temporary and permanent seismic networks (e.g. Angus et al., 2006; Sodoudi et al., 2006, 2015; Gök et al., 2007, 2015; Vanacore et al., 2013; Vinnik et al., 2014). Interpretations from these studies are either confined to a limited region or to a limited depth extent, i.e., to crustal depths only. Thus, the variations of lithospheric thickness have not yet been homogeneously characterized in Turkey and surroundings. A robust estimate of the lithospheric thickness is an important constraint for our understanding of mantle deformation in response to tectonic forces (see Fischer et al., 2010 and Jones et al., 2010 for reviews). In the present study, we provide a complete image of the LAB topography below Anatolia and adjacent regions based on a combination of data from several different networks in the area. To achieve this, we have employed the S-receiver function technique, which is particularly suited to identify seismic discontinuities in the upper mantle, especially when low-velocity zones are involved.

2 Tectonic Setting

The Cenozoic closure of the Tethys Ocean and the following continental collision of the northward moving African and Arabian plates with the Eurasian plate are considered to be the main driving processes of the present tectonic setting in the eastern Mediterranean and Anatolia (Şengör and Kidd, 1979; Dewey and Şengör, 1979; Taymaz et al., 1990, 1991a,b; Jackson et al., 1992; Armijo et al., 1999; Taymaz et al., 2004; Faccenna et al., 2014; Schildgen et al.; 2014). Fig. 1 summarizes the tectonic setting of the target area. GPS measurements have highlighted that the retreating Hellenic trench and associated slab roll-back of the subducting African lithosphere are currently the major driving forces for the western movement of the Anatolian plate (e.g. McKenzie, 1978; Reilinger et al., 2006). Current deformation is mainly accommodated through strain localization along the North Anatolian Fault (NAF) and the East Anatolian Fault (EAF). The deformation along the EAF is purely left lateral with no compressional component except for localized thrust ridges associated with strike-slip tectonics (Bulut et al., 2012). Body wave tomography images on global and regional scale indicate that the Hellenic subduction penetrates down to the lower mantle with an average dip of about 40° (Wortel and Spakman, 2000; Faccenna et al., 2006; Biryol et al., 2011; Salaün et al., 2012) while a recent waveform tomography study by Fichtner et al. (2013a,b) did not report any deep slab.

Crustal thickness ranges from 35 to 40 km along the North Anatolian Fault and shallows to 25-30 km in the Sea of Marmara region based on receiver functions and controlled source studies (Saunders et al., 1998; Sato et al., 2004; Zor et al., 2006; Laigle et al., 2008; Özacar et al., 2008; Bécel et al., 2009, 2010; Vanacore et al., 2013; Karabulut et al., 2013; Sodoudi et al., 2015). The lithosphere-asthenosphere boundary beneath the East Anatolian Accretionary Complex (EAAC) has been observed at 60-80 km depth based on S-receiver functions (Angus et al., 2006). They consider this lithospheric thickness to be anomalously thin and interpret this structure to be the remnant of the detachment of an oceanic slab. Further evidence for a thin lithosphere overlying hot and partially molten asthenospheric material beneath Eastern Anatolia has been found in other P- and S-receiver function images (Zor et al., 2003; Özacar et al., 2008; Vanacore et al., 2013). Other indications of a shallow LAB are strong attenuation of Lg and Sn phases (Gök et al., 2003) and relatively low Pn- and uppermost mantle S-velocities (Al-Lazki et al., 2004, Maggi and Priestley, 2005). The slow velocity anomaly was attributed to the ascending asthenosphere that is emplaced beneath the plateau following the detachment of the northward subducting Arabian oceanic lithosphere (Keskin, 2003; Faccenna, 2003; Şengör et al., 2003; Biryol et al., 2011; Fichtner et al., 2013a,b). Recently, tomography studies by Biryol et al. (2011) and Fichtner et al. (2013a) have confirmed that a hot and buoyant asthenospheric body supports the ~2 km elevation of the Eastern Anatolian Plateau in the presence of an about 45 km thick crust (Şengör et al., 2003; Zor et al., 2003). At about 350 km depth, a fast anomaly has been found by tomographic studies and interpreted to represent a slab detachment (Lei and Zhao, 2007 and Zor, 2008).

3 Data and Method

Recent extensions of seismic and geodetic networks in Turkey have considerably contributed to our understanding of seismicity patterns and crustal and lithospheric structures beneath Anatolia and the surrounding regions. These developments have been triggered in particular by the destructive 1999 Izmit (Mw 7.4) and Düzce (Mw 7.2) earthquakes. Our data set consists of teleseismic waveforms that were extracted from 1028 earthquakes recorded at 195 broadband stations (Fig. 2), operated by Kandilli Observatory and Earthquake Research Institute (KOERI; Kalafat et al., 2008), NOA-Net, Aristotle University Thessaloniki (HT-Net) and GEOFON (Hanka

and Kind, 1994; GEOFON Data Centre, 1993).

We apply the S-receiver function method to this dataset in order to image seismic discontinuities in the crust and upper mantle. A description of the S-receiver function analysis scheme and examples are found in Yuan et al. (2006) and Kind et al. (2012, 2014). The method employs teleseismic S phases, which are converted to P waves at a discontinuity below the station site.The main advantage of this approach over the P-receiver function technique is that there is practically no interference from multiples, which can otherwise significantly interfere with the imaging of deeper convertors, in particular for the depth range of 80-200 km in continental regions. S-receiver functions provide a broad sampling of the upper mantle comparable to the steep angle reflection images of the crust. This technique requires a sufficient number of high quality observations of teleseismic S phases, typically at least about 60 records per station with signal-to-noise ratio above two. Permanent broadband stations or densely deployed temporary broadband networks can usually provide this amount of data. The limit of resolution is determined by the frequency content of teleseismic S phases, which usually only give convincing results for periods longer than a few seconds. Since the essential part of S-receiver functions consists of weakly converted P-precursors of the SV phase, the signal-to-noise ratio needs to be improved by stacking large number of records at the same station, or within a confined region of conversion points at a fixed depth, or by migrating the rays into the depth domain based on a 1D reference model and the assumption that conversions occur at horizontal boundaries. The latter approach is known as a common-conversion-point stack (CCP). To reduce source side effects, the distribution of sources should have a well-balanced azimuthal and epicentral coverage. In general, events at epicentral distances between 60° and 85° are suitable for S-receiver function studies. Reviews of the application of the S-receiver function technique in investigations of the lithosphere-asthenosphere boundary are found in Rychert and Shearer (2009), Fischer et al. (2010) and Rychert et al. (2010). More recently, further studies of upper mantle discontinuities have been published by Levander and Miller (2012), Kumar et al. (2012a,b), Hopper et al. (2013), Kind et al. (2013) and Sodoudi et al. (2013).

We have restricted the dataset by visual inspection to reasonably simple and clear waveforms. Deconvolution results that fail to transform the SV signal (Q component) into a sharp spike, have also been excluded based on a further visual inspection. This resulted in 11660 S-receiver functions. For initial evaluation, all traces are combined within non-overlapping 0.5° epicentral distance bins irrespective of the station and source locations (Fig. 3). This figure shows all observable precursors of the S phases, including phases that might disturb the expected S-to-P conversion from upper mantle discontinuities below the stations. A positive conversion (red) at -3 s, corresponding to the Moho, and a negative (blue) signal at -10 s, interpreted as the LAB, are clearly visible. We can also identify the SKS660p and ScS660p phases caused by S-to-P conversions of SKS and ScS at the 660 km discontinuity. These signals have significantly different slowness compared to the S-to-P conversions of the S phase at the LAB or Moho, meaning that they cut across all other phases before the S signal. It means that, if we apply proper delays before summation according to the slowness of the converted S phase, all other phases traveling with different slowness are suppressed. The strong signal following S is the SPn phase, which is caused by an S-to-P conversion traveling horizontally as a P wave through the uppermost mantle layer at the receiver side.

4 Synthetic tests for imaging inclined structures with S-receiver functions

Since we expect to image in the south of the study region an inclined slab, we first use synthetic seismograms to quantify the magnitude of artifacts which may occur during the depth transformation of the time domain records and infer the maximum range of inclination at which the LAB of a slab can be imaged using S-receiver functions. Figs.4a-f show synthetic seismograms

calculated with the RAYSUM software (Frederiksen and Bostock, 2000), which is capable of calculating receiver functions for inclined layers. In these figures, the converters used for the forward modeling are displayed by black lines. Positive and negative amplitudes of the synthetic S-RFs (S-receiver functions) are shown by red and blue, respectively. Based on available reference tomographic models (e.g. Biryol et al., 2011; Bakirci et al., 2012), an inclined 45 km thick high velocity zone (slab) dipping to the north is used as the input model. The modeling has been performed for inclination angles between 0° and 50° with an increment of 10°. The velocity contrasts are from 8.0 km/s to 7.5 km/s at the lower boundary of the slab and from 6.5 km/s to 8.0 km/s at its upper boundary, as depicted in Fig. 4a. S-RF traces are modeled for back azimuths from 0° to 180° with an increment of 10° and for a constant slowness of 9.8 s/° which corresponds to an epicentral distance of 80°. Events with back azimuths from 180°-360° would yield identical information to that obtained for the range 0°-180° due to the 180°-periodicity of RFs for inclined structures. Fig. 4g shows the incidence angle of the incoming S wave at the lower boundary of the dipping slab as a function of the back azimuth. For zero and small incidence angles of the high velocity zone, the discontinuities are properly imaged at expected positions (see Figs.4a,b). A signal is generated by events from nearly all azimuths. For a slab inclination greater than 20°, the lower boundary of the slab is imaged only by events from southern directions since for back azimuths of 90° the emergent angle of the converted Sp wave reaches its critical value (see green line in Fig. 4g). Thus, for events from northern azimuths (0°-90°), no transmitted Sp conversion exists. For larger inclinations of the slab, the back azimuthal range for which Sp converted energy is transmitted becomes even smaller (see Fig. 4d-f and red, yellow and violet lines in Fig. 4g). Moreover, the amplitudes from the inclined structure show a reversal for slab inclinations larger than 30° and events from southern directions (160°-180°). This amplitude reversal occurs similarly for the Q-component of P-RFs from inclined structures (Schneider et al., 2013) and might cause destructive interference in CCP stacks.

5 Observations and interpretation

We extracted several north-south and east-west profiles through Anatolia. The results from time domain stacks and depth transformations are shown in Figs. 5-10. The receiver functions are filtered with an 8 s low-pass filter in those figures. In the time domain, a move-out correction is applied using a reference slowness of 6.4 s/° and time-corrected traces are stacked for S-to-P piercing points at 200 km depth within a certain window of latitude and longitude along the selected profiles. We chose the piercing point depth of 200 km in the time domain images in order to focus on potentially subducting structures. The summation windows have been placed along east-west and north-south profiles. The size of the windows is 0.3° in the north-south (or east-west) direction and the width of the section in the east-west (or north-south) direction given in each figure caption (e.g. Fig. 5). Neighboring boxes are not overlapping, i.e., no lateral smoothing is applied along the profiles. The relatively large profile widths (3-9°) were required to collect a sufficient number of traces to ensure a good signal-to-noise ratio of the originally weakly converted phases in the summation trace. In order to obtain an image directly in the depth-distance domain, we also calculated CCP stacks, which, unlike the time domain summation, does not require the arbitrary choice of a piercing point depth. We assumed the IASP91 global reference model for the time-to-depth conversion. The receiver function depth transformation technique does not depend strongly on the given velocity model. The same profile width as in the time domain technique is used in the depth transformation technique and all rays traveling within the profile width at any depth are summed. This means that, generally more traces contribute to each profile in the depth domain because for the time-domain images only rays with piercing points in a particular depth are summed.

5.1 Moho

A positive converter associated with the Moho is very obvious in all profiles in Figs. 5-10. The Moho is only briefly discussed here as it is not the main target of this study. Basically, shorter period P-receiver functions are more suitable for a detailed image of the Moho or intracrustal discontinuities. However, we point out a few crustal observations obtained from S-receiver functions. The crustal thickness increases from the Aegean to Eastern Anatolia from ~25 km to ~40 km (see Fig. 9). As the seismic traces are averaged with piercing points in relatively large grids (1° longitude, 4° latitude in Fig. 9), small-scale variations of the Moho are not well-resolved. The observed range of the Moho depths is consistent with results from previous receiver function studies (e.g. Saunders et al., 1998; Zor et al., 2006; Özacar et al., 2008; Vanacore et al., 2013; Karabulut et al., 2013). However, in Eastern Anatolia, Şengör et al. (2003) and Zor et al. (2003) reported that the Moho depth increases from less than 40 km at the Bitlis Suture to about 50 km near the Black Sea. This deep Moho is not seen in our data (Fig. 7), implying that this change in Moho depth only occurs in a limited region, such that it is not visible in our relatively large-scale north-south profile in Fig. 7. Vanacore et al. (2013) presented a detailed Moho map from P-receiver functions. They also observed a general increase in Moho depth from west to east, which is roughly consistent with our S-RF results. The subducting African Moho is visible to a depth of nearly 100 km in the southern part of western Anatolia and the Aegean (Fig. 5a). No significant change in Moho depth is visible across the North Anatolian Fault in the south-north profiles (see e.g. Fig. 6). However, our data are filtered with an 8 s low-pass filter and therefore not optimized for higher resolution determination of the Moho depth across the NAF. P-receiver functions are more useful for this purpose.

5.2 Lithosphere-asthenosphere boundary

The stacked S-RF images in Figs. 5-10 show a clear observation of a relatively homogeneous negative discontinuity at 80-100 km depth beneath the entire region, which we interpret to represent the LAB. This signal is not a sidelobe of the Moho for the following reason. Seismic signals are causal, i.e. there is no signal in the unfiltered records before the arrival time. We found LAB signals in unfiltered and undeconvolved traces in the same depth range as in filtered and deconvolved traces (see Fig.11A), which proves that they correspond to a physical discontinuity The smooth appearance of the LAB in Figs. 5-10 is due to the chosen filter (8 s low-pass). Using shorter wavelengths or no filter, the LAB dissolves into several discontinuous signals (see Fig. 11A). More such examples in North America are shown in the final version of Kind et al. (2015). Such a laminated structure of the mantle lithosphere in western Europe ha been known for a long time from long range controlled source experiments (e.g. Kind, 1974). The new receiver function data seem to confirm the laminated structure. We conclude that the bottom of the lithosphere consists of several neighboring laterally and vertically limited discontinuities with decreasing velocity downward. The vertical extent of the laminated region is up to 50 km (Fig.11A). Due to the superposition of neighboring signals, the depth and amplitudes of the longer period filtered LAB depend on the period. We have chosen this relatively long period filter to emphasize the dominant structures in the mantle as clearly as possible. The Moho and the 410 and 660 discontinuities have different characteristics and get sharper when shorter periods are used, indicating that they are simple first order discontinuities.

Our observations of a shallow LAB beneath Anatolia confirm earlier results. Previous findings mainly from body and surface wave tomography studies (Biryol et al., 2011; Bakirci et al., 2012; Salaün et al., 2012; Fichtner et al., 2013a,b) indicate a similarly thin lithosphere beneath entire Anatolia. Additional constraints confirming a thin lithosphere are provided by the much smaller-

scale P-RF and S-RF images in Sodoudi et al. (2006, 2015), Angus et al. (2006), Özacar et al. (2008) and Gök et al. (2011). Sodoudi et al. (2006) found the northern Aegean LAB near 150 km depth. Additional indications of a thin lithosphere are strong Lg and Sn attenuation observations (Gök et al., 2003), and relatively low S- and Pn-wave velocity anomalies (e.g. Maggi and Priestley, 2005, Gök et al., 2007; Al-Lazki et al., 2004). A joint analysis of surface wave group velocities (Rayleigh and Love waves) and teleseismic receiver functions suggests that the average LAB depth is about 90 km in the Arabian Plate and about 70 km in the Anatolian Block (Gök et al., 2007).

However, our observations of the thin lithosphere provide seismological support for the removal of lithosphere beneath entire Anatolia. Indications of lithospheric removal in the region have been given in earlier regional tomography studies (i.e. Wortel and Spakman, 2000; Piromallo and Morelli, 2003). Şengör et al. (2003) proposed the detachment of the Arabian plate and subsequent upwelling of asthenospheric mantle to explain the high elevation and the lack of a thick mantle lithosphere beneath the Eastern Anatolian Plateau.

5.3 Subduction of African lithosphere

In our stacked S-RFs and corresponding depth migrated images, the African LAB dips flatly to the north with an angle of 20-30° and reaches down to almost 150 km depth beneath Anatolia and the Aegean (Figs. 5 and 6). This is similar to the observed slab geometry found by a recent Rayleigh wave tomography by Bakirci et al. (2012). It is also similar to receiver function results from Li et al. (2003) and Sodoudi et al. (2006, 2015). In contrast to that, the African slab observed with tomographic methods reaches into the lower mantle with a dip of 40-50° (e.g. Wortel and Spakman, 2000). What is the reason for the differences in the observations of the two types of data? Comparing our data with the synthetics in Fig. 4, we realize that for a slab dip >40° only events with a back azimuth between 160-200° would contribute to the slab images. However, we have only very few events from the south (see Fig. 2). A steep part of the slab is thus not expected to show on our images, and its absence on our image does not rule out the presence of a deeper slab. Fig. 4 also shows that slabs with a dip of 20-30° can be observed relatively well with S-receiver functions. All our images of the subducting African plate are only obtained from the shallow and flat dipping part of the slab. Features of slab break-off were inferred later from teleseismic tomography images (Lei and Zhao, 2007; Zor, 2008). Without requiring slab break-off models, recent geodynamic models (Göğüş and Pysklywec, 2008; Komut et al., 2012; Göğüş, 2014) associate present-day high topography, lithospheric thinning and hot surface heat flow with vertical flow and very high thermal conditions (e.g. 1300-1400 °C) of the uppermost mantle that resulted in the delamination of lithosphere, which was originally proposed by Bird (1979) for the Colorado Plateau.

Biryol et al. (2011) observed a wide gap between the high velocity anomalies of the subducting Hellenic and Cyprus slabs, which they interpreted as slab tear. Our north-south profile at the transition of the Hellenic and Cyprus slabs (Fig. 6) is too broad to resolve such a slab tear. The dipping features of the African Moho along the Hellenic and Cyprus trenches differ, implying that the subduction is only shallow toward the south of Cyprus (Figs. 5, 6). The absence of trench-perpendicular extension on the over-riding central Anatolia is different from the western Anatolia and the Aegean and was previously considered to be the consequence of a lower subduction angle of the African slab along the Cyprus trench (Barka and Reilinger, 1997). Changing slab geometry with decreasing dip angle from west to east was previously suggested to result from the Eratosthenes seamount beneath Cyprus resisting subduction (Kempler and Ben-Avraham, 1987; Barka&Reilinger, 1997). The east-west profile along the southern boundary of Anatolia (Fig. 8) provides more detailed information. Here, we see that the African (or Hellenic) slab is apparently dipping to the east towards Cyprus where it reaches about 150 km depth; this geometry can be

interpreted as a northward-directed dip of the African Plate, resulting in a structural boundaries that are inclined to the north and east. To the east of Cyprus, we see the flat Arabian LAB near 100 km depth (Fig. 8), clearly discontinuous with the African slab LAB. This transition occurs significantly west of the Dead Sea Transform Fault (which is at 35-36°E, see Fig. 1), which might indicate that the Dead Sea Transform Fault is inclined to the west.

5.4 Depth of the NAF

The depth extent of the lithosphere across the NAF is still a controversial issue. Biryol et al. (2011) found a sharp velocity contrast across the NAF reaching down to 100-150 km depth. Fichtner et al. (2013b) identified a narrow low velocity zone reaching about 100 km depth and interpreted it as a zone of weakness. However, Salaün et al. (2012) did not find any evidence for a lithosphere penetrating NAF in a surface wave study, inverting fundamental-mode Rayleigh wave phase velocity maps. Similarly, we also do not observe any significant contrast in the delay times of the LAB signals across the NAF (Fig. 6). We conclude therefore that lithospheric depths and average velocities are very similar on both side of the fault. We also tested narrower north-south profiles and obtained similar results, although the data quality worsens when fewer traces are summed. The oblique pattern of the fast polarization direction inferred from the SKS measurements relative to the actual orientation of the NAF is an indication that the NAF is a relatively shallow feature not linked to a deep deformation zone (e.g. Paul et al., 2014). These observations are different from those found in northeast Tibet (Leon Soto et al., 2012; Eken et al., 2013) where fast anisotropy directions within the entire lithosphere are nearly parallel to the strike of the North and South Kunlun faults. In contrast to northern Anatolia, significant differences in crustal and lithospheric thickness are observed across the San Andreas Fault in southern California based on P- and S-receiver functions (Lekic et al., 2011; Miller et al., 2014).

5.5 Mantle transition zone discontinuities

We observed the 410 discontinuity beneath most of Anatolia. This discontinuity is shallowest beneath Western Anatolia at ~390 km depth and deepens smoothly towards central Anatolia to 420 km. The depth is approximately constant below central Anatolia and deepens again across eastern Anatolia from 410 to 430 km (Fig 9). The reason for the lateral variation of the 410 depth in Fig.9 are probably the lateral velocity variations in the sub-lithospheric mantle, because the LAB itself is flat. Large temperature variations across Anatolia in the transition zone, which would cause an actual deflection of the 410 depth, seem less likely. We leave studies of the upper mantle discontinuities to a future analysis using P-receiver functions that are more suitable for this purpose. In the context of this study, these observations are mainly used to verify the reliability of our data. Another observation is a negative, but more scattered discontinuity about 50 km above the 410 in the entire area. Such a discontinuity is known globally (Tauzin et al., 2010) and considered to be caused by a low velocity layer containing liquids or partial melts. We do not observe any other prominent discontinuity between the LAB and the low velocity zone on top of the 410 on larger scale, especially no clear indications for the Lehmann discontinuity, which has been observed below the north-western United States (Kind et al., 2015) and large parts of Scandinavia (Kind et al., 2013) using S-receiver functions.

6 Conclusions

The depth of the LAB beneath the entire region of Anatolia varies between 80-100 km, and in particular does not change when crossing the North Anatolian and East Anatolian Fault Zones. This indicates that the thickness of the lithosphere is similar beneath Anatolia and the neighboring edges of the Eurasian and Arabian plates. An exception is the lithospheric thickness near 150 km in the northern Aegean (Sodoudi et al. 2006). In southern Anatolia, the subducting African lithosphere

(LAB) between the Aegean and west Cyprus is imaged down to a depth of about 150 km, dipping to the north and east. Synthetic seismogram calculations have shown, that a steeper dipping deeper slab would not have been imaged by S receiver functions, however. To the east of Cyprus a shallow LAB is observed (similar to the Arabian LAB) with apparently no indication of African subduction.

Acknowledgements

This research was supported by the Deutsche Forschungsgemeinschaft. We thank the Kandilli Observatory and Earthquake Research Institute, National Earthquake Monitoring Center (KOERI-NEMC), Turkey, Aristotle University Thessaloniki (HT-Net), Greece, National Observatory of Athens (NOA), Greece and the GEOFON Data Center at the GFZ Potsdam, Germany, for their efforts in maintaining free public access of digital recordings to the scientific community. T. Eken was funded by a Humboldt Research Fellowship for Postdoctoral Researchers provided by the Alexander von Humboldt Foundation. T. Taymaz thanks National Scientific and Technological Research Council of Turkey (TÜBİTAK), Turkish Academy of Sciences (TÜBA) in the framework for Young Scientist Award Program (TT-TÜBA-GEBİP 2001-2-17), and the Alexander von Humboldt Foundation Research Fellowship Award for financial support. We thank Jim Mechie and Eric Sandvol for reading the manuscript and for helpful comments. We also thank Andrew Frederiksen for providing the RAYSUM code used in the synthetic RF calculations.

References

Al-Lazki, A. I., Seber, D., Sandvol, E., Turkelli, N., Mohamad, R. and Barazangi, M.: Tomographic Pn velocity and anisotropy structure beneath the Anatolian plateau (eastern Turkey) and the surrounding regions, Geophys. Res. Lett., 30(24), 8043, doi:10.1029/2003GL017391, 2004.

Angus, D., Wilson, D., Sandvol, E. and Ni, J.: Lithospheric structure of the Arabian and Eurasian collision zone in eastern Turkey from S-wave receiver functions, Geophys. J. Int., 166, 1335–1346, doi:10.1111/j.1365-246X.2006.03070.x, 2006.

Armijo, R., Meyer, B., Hubert, A. and Barka, A.: Westward propagation of the North Anatolian fault into the northern Aegean: Timing and kinematics, Geology, 27(3), 267–270, 1999.

Bakirci, T., Yoshizawa, K. and Özer, M.F.: Three-dimensional S wave structure of the upper mantle beneath Turkey from surface wave tomography. Geophys. J.Int.190, 1058–1076, 2012.

Barka, A. and Reilinger, R.: Active tectonics of the eastern Mediterranean region: deduced from GPS, neotectonic and seismicity data. Annali di Geofisica XL 3, 587-610, 1997.

Bécel, A., Laigle, M., de Voogd, B., Hirn, A., Taymaz, T., Galvé, A., Shimamura, H., Murai, Y., Lépine, J.-C., Sapin, M. and Özalaybey, S.: Moho, Crustal Architecture and Deep Deformation Under the North Marmara Trough, from the SEISMARMARA Leg-1 Offshore-Onshore Reflection-Refraction Survey, Tectonophysics, 467, 1-21, . doi:10.1016/j.tecto.2008.10.022, 2009.

Bécel, A., Laigle, M., de Voogd, B., Hirn, A., Taymaz, T., Yolsal-Çevikbilen, S. and Shimamura, H.: North Marmara Trough architecture of basin infill, basement and faults, from PSDM reflection and OBS refraction seismics, Tectonophysics, 490, 1-14, doi:10.1016/j.tecto.2010.04.004, 2010.

Bird, P.: Continental delamination and the Colorado Plateau: Journal of Geophysical Research, v. 84, p. 7561–7571, doi:10.1029/JB084iB13p07561, 1979.

Bird, P.: An updated digital model of plate boundaries, Geochemistry Geophysics Geosystems, 4(3), 1027, doi:10.1029/2001GC000252, 2003.

Biryol, C.B., Beck, S.L., Zandt, G. and Özacar, A.A.: Segmented African lithosphere beneath the Anatolian region inferred from teleseismic P-wave tomography. Geophys. J. Int. 184, 1037–1057, 2011.

Bulut, F., Bohnhoff, M., Eken, T., Janssen, C., Kl, T., Dresen, G.: The East Anatolian Fault Zone: Seismotectonic setting and spatiotemporal characteristics of seismicity based on precise earthquake locations. J. Geophys. Res. B: Solid Earth, 117 (7), art. no. B07304, 2012.

Dewey, J.F. and Şengör, A.M.C.: Aegean and surrounding regions: Complex multiplate and continuum tectonics in a convergent zone. Geological Society of America Bulletin 90, 84–92. doi:10.1130/0016-7606, 1979.

Eken, T., Tilmann, F., Mechie, J., Zhao, W.J., Kind, R., Su, H.P., Xue, G.Q. and Karplus, M.: Seismic Anisotropy from SKS Splitting beneath Northeastern Tibet. Bull. seism. Soc. Am., 103 (6) 3362-3371, DOI: 10.1785/0120130054, 2013.

Faccenna, C., Jolivet, L., Piromallo, C. and Morelli, A.: Subduction and the depth of convection in the Mediterranean mantle, J. Geophys. Res., 108(B2), 2099, doi:10.1029/2001JB001690, 2003.

Faccenna, C., Bellier, O., Martinod, J., Piromallo, C. and Regard, V.: Slab detachment beneath Eastern Anatolia: A possible cause for the formation of the North Anatolian fault, Earth Planet. Sci. Lett., 242, 85–97, doi:10.1016/j.epsl.2005.11.046, 2006.

Faccenna,C., Becker, T. W., Auer, L., Billi, A., Boschi, L., Brun, J.P., Capitanio, F.A., Funiciello, F., Horvath, F., Jolivet, L., Piromallo, C., Royden, L., Rossetti, F. and Serpelloni, E.: Mantle dynamics in the Mediterranean. Reviews of Geophysics, doi: 10.1002/2013RG000444, 2014.

Fichtner, A., Saygin, E., Taymaz, T., Cupillard, P., Capdeville, Y. and Trampert, J.: The deep structure of the North Anatolian Fault Zone. Earth Planet. Sci. Lett. 373, 109–117, 2013a.

Fichtner, A., Trampert, J., Cupillard, P., Saygin, E., Taymaz, T., Capdeville, Y. and Villasenor, A.: Multiscale full waveform inversion, Geophys. J. Int. doi: 10.1093/gji/ggt118, 2013b.

Fischer, K.M., Ford, H.A., Abt, D.L. and Rychert, C.A.: The lithosphere asthenosphere boundary. Annual Review of Earth and Planetary Sciences 38, 551–575 doi:10.1146/annurev-earth-040809-152438, 2010.

Frederiksen, A.W. and Bostock, M.G.: Modelling teleseismic waves in dipping anisotropic structures. Geophys. J. Int. 141, 401–412, 2000.

Gans, C.R., Beck, S.L., Zandt, G., Biryol, C.B. and Özacar, A.A.: Detecting the limit of slab break-off in Central Turkey: new high-resolution Pn tomography results, Geophys. J. Int., 179, 1566–1572, 2009.

GEOFON Data Centre: GEOFON Seismic Network. Deutsches GeoForschungsZentrum GFZ. doi:10.14470/TR560404, 1993.

Göğüş, O. H., and Pysklywec, R.N.: Mantle lithosphere delamination driving plateau uplift and synconvergent extension in eastern Anatolia, Geology, 36, 723–726, doi:10.1130/G24982A.1, 2008.

Göğüş, O.H.: Rifting and subsidence following lithospheric removal in continental back arcs, Geology, doi:10.1130/G36305.1, 2014.

Gök, R., Sandvol, E., Törkelli, N., Seber, D. and Barazangi, M.: Sn attenuation in the Anatolian and Iranian plateau and surrounding regions, Geophys. Res. Lett., 30(24), 8042, doi: 10.1029/2003GL018020, 2003.

Gök, R., Pasyanos, M. and Zor, E.: Lithospheric structure of the continent-continent collision zone: Eastern Turkey, Geophys. J. Int., 169, 1079–1088, doi:10.1111/j.1365-246X.2006.03288.x, 2007.

Gök, R., Mellors, R.J., Sandvol, E., Pasyanos, M., Hauk, M., Takedatsu, R., Yetirmishli, G., Teoman, U., Turkelli, N., Godoladze, T. and Javakishvirli, Z., : Lithospheric velocity structure of the Anatolian plateau-Caucasus-Caspian region, J. Geophys. Res., 116, B05303, doi:10.1029/2009JB000837, 2011.

Hanka, W., and Kind, R.: The GEOFON Program. Annals of Geophysics, 37(5). doi:10.4401/ag-4196, 1994.

Hopper, E., Ford, H.E., Fischer, K.M. and Lekic, V.: The lithosphere-asthenosphere boundary and the tectonic-magmatic history of the northwestern United States, Earth Planet Sci. Lett., doi.org/10.1016/j.epsl.2013.12.016, 2013.

Jackson, J., Haines, A. J. and Holt, W. E.: The horizontal velocity field in the deforming Aegean region determined from seismic moment tensors of earthquakes, J. Geophys. Res., 97, 17,657–17,684, doi:.10.1029/92JB01585, 1992.

Jones, A. G., Plomerova, J., Korja, T., Sodoudi, F. and Spakman, W.: Europe from the bottom up: A statistical examination of the central and northern European lithosphere-asthenosphere boundary from comparing seismological and electromagnetic observations, Lithos, 120, 14–29, 2010.

Kalafat, D., Kekovali, K., Kilic, K. et al.: An Earthquake Catalog for Turkey and the Surrounding Area (M≥3.0; 1900-2008), Kandilli Observatory and DAE, UDIM, Istanbul, (in Turkish), 2008.

Karabulut, H., Paul, A., Ergun, T.A., Hatzfeld, D., Childs, D.M. and Aktar, M.: Long-wavelength undulations of the seismic Moho beneath the strongly stretched Western Anatolia. Geophys. J. Int., 194, 450–464, 2013.

Kempler, D and Ben-Avraham, Z.: The tectonic evolution of the Cyprean arc, Annales Tectonicae, 1, 58-71, 1987.

Keskin, M.: Magma generation by slab steepening and breakoff beneath a subduction-accretion complex: An alternative model for collision-related volcanism in Eastern Anatolia, Turkey,

Geophys. Res. Lett., 30(24), 8046, doi:.10.1029/2003GL018019, 2003.

Kind, R. (1974), Long range propagation of seismic energy in the lower lithosphere, J. Geophys. 40, 189-202.

Kind, R., Yuan, X. and Kumar, P.: Seismic receiver functions and the lithosphere-asthenosphere boundary, Tectonophysics, 536–537, 25–43, 2012.

Kind, R., Sodoudi, F., Yuan, X., Shomali, H., Roberts, R., Gee, D., Eken, T., Bianchi, M,. Tilmann, F., Balling, N., Jacobsen, B.H., Kumar, P. and. Geissler, H.W.: Scandinavia: A former Tibet? Geochem. Geophys. Geosyst 14, 4479–4487, doi:10.1002/ggge.2025, 2013.

Kind, R., Yuan, X. , Mechie,J. and Sodoudi, S.: Structure of the upper mantle in the north-western and central United States from USArray S-receiver functions. Solid Earth, in review, 2015.

Komut, T., Gray, R., Göğüş, H.O. & Pysklywec, R. N., 2012. Mantle Flow Uplift of Western Anatolia and the Aegean: Interpretations from Geophysical Analyses and Geodynamic Modelling, J. Geophys. Res., 117, B11412. doi:10.1029/2012JB009306.

Kumar, P., Yuan, X., Kind, R. and Mechie, J.: The lithosphere-asthenosphere boundary observed with USArray receiver functions. Solid Earth 3, 149-159, doi:10.5194/se-3-149, 2012a.

Kumar, P., Kind, R., Yuan, X. and Mechie, J.: USArray receiver function images of the LAB, Seismol. Res. Lett., 83, 486–491, doi:10.1785/gssrl.83.3.486, 2012b.

Laigle, M., Becel, A., de Voogd, B., Hirn, A., Taymaz, T.and Ozalaybey, S.: A first deep seismic survey in the Sea of Marmara: Deep basins and whole crust architecture and evolution, Earth Planet Sci. Lett., 270, 168–179, 2008.

Lei, J. and Zhao, D.: Teleseismic evidence for a break-off subducting slab under eastern Turkey, Earth Planet. Sci. Lett., 257, 14–28, 2007.

Lekic, V., French, S. W. and Fischer, K. M.: Lithospheric thinning beneath rifted regions of southern California, Science, 334 (6057), 783–787, doi:10.1126/science.1208898, 2011.

Leon Soto, G., Sandvol, E., Ni, J.F., Flesch, L.M., Hearn, T.M., Tilmann, F., Chen, Y.J. and Brown, L.: Significant and vertically coherent seismic anisotropy beneath eastern Tibet, J. Geophys. Res., 117, B05308, doi:.10.1029/2011JB008919, 2012.

Levander, A. and Miller, M.S.: Evolutionary aspects of lithosphere discontinuity structure in the western U.S. Geochem. Geophys. Geosyst., 13, Q0AK07, doi:10.1029/2012GC004056, 2012.

Li, X., Bock,G., Vafidis, A., Kind, R., Harjes, H.-P., Hanka, W., Wylegalla, K., van der Meijde, M., and Yuan, X.: Receiver function study of the Hellenic subduction zone: imaging crustal thickness variations and the oceanic Moho of the descending African lithosphere, Geophys. J. Int. 155, 733-748, 2003.

Maggi, A., and Priestley, K.: Surface waveform tomography of the Turkish–Iranian Plateau, Geophys. J. Int., 160, 1068–1080, 2005.

McKenzie, D.: Active tectonics of the Alpine—Himalayan belt: the Aegean Sea and surrounding regions. Geophys. J. R. Astr. Soc., 55(1), 217-254, 1978.

Miller, S.M., Zhang, P. and Dolan, J.F.: Moho structure across the San Jacinto fault zone: Insights into strain localization at depth. Lithosphere 6 (1), 43-47, doi: 10.1130/l295.1, 2014.

Okay, A.I., and Satır, M.: Coeval plutonism and metamorphism in a latest Oligocene metamorphic core complex in northwest Turkey: Geological Magazine, v. 137, p. 495–516, 2000.

Özacar, A. A., Gilbert, H. and Zandt, G.: Upper mantle discontinuity structure beneath East Anatolian Plateau (Turkey) from receiver functions, Earth Planet. Sci. Lett., 269, 427–435, doi:.10.1016/j.epsl.2008.02.036, 2008.

Paul, A., Karabulut, H., Mutlu, A.K. and Salaun, G.: A comprehensive and densely sampled map of shear-wave azimuthal anisotropy in the Aegean-Anatolia region, Earth Planet. Sci. Lett., 389, 14-22, DOI: 10.1016/j.epsl.2013.12.019, 2014.

Piromallo, C., and Morelli, A.: P-wave tomography of the mantle under the Alpine-Mediterranean area: Journal of Geophysical Research, v. 108, 2065, doi:10.1029/2002JB001757, 2003.

Reilinger, R., McClusky, S., Vernant, P., et al.: GPS constraints on continental deformation in the Africa–Arabia–Eurasia continental collision zone and implications for the dynamics of plate interactions, J. Geophys. Res., 111, B05411, doi:.10.1029/2005JB004051, 2006.

Rychert, C. A., and Shearer, P. M.: A global view of the lithosphere-asthenosphere boundary, Science, 324, 495–498, doi:10.1126/science.1169754, 2009.

Rychert, C. A., Shearer, P. M. and Fischer, K. M.: Scattered wave imaging of the lithosphere–asthenosphere boundary, Lithos, 120, 173–185, 2010.

Salaün, G., Pedersen, H. A., Paul, A., Farra, V., Karabulut, H., Hatzfeld, D., Papazachos, C., Childs, D. M., Pequegnat, C. and SIMBAAD Team: High-resolution surface wave tomography beneath the Aegean-Anatolia region: Constraints on upper-mantle structure, Geophys. J. Int., 190(1), 406–420, doi:10.1111/j.1365-246X.2012.05483.x, 2012.

Sato, T., Kasahara, J., Taymaz, T. et al.: A study of microearthquake seismicity and focal mechanisms within the Sea of Marmara (NW Turkey) using ocean-bottom seismometers (OBS), Special Issue of Tectonophysics, 391, 303-314, doi:10.1016/j.tecto.2004.07.018, 2004.

Saunders, P., Priestley, K. and Taymaz, T.: Variations in the crustal structure beneath western Turkey, Geophys. J. Int., 134, 373–389, 1998.

Schildgen, T.F., Yildirim, C., Cosentino D. and Strecker, M.R.: Linking slab break-off, Hellenic trench retreat, and uplift of the Central and Eastern Anatolian plateaus. Earth-Science Reviews 128, 147-168, doi.org/10.1016/j.earscirev.2013.11.006, 2014.

Schneider, F. M., Yuan, X., Schurr, B., Mechie, J.,Sippl, C., Haberland, C., Minaev, V., Oimahmadov, I., Gadoev, M., Radjabov, N., Abdybachaev, U., Orunbaev, S., and Negmatullaev, S.: Seismic imaging of subducting continental lower crust beneath the Pamir. Earth Planet. Sci.

Lett. 375, 101–112, 2013.

Sodoudi, F., Kind, R., Hatzfeld, D., Priestley, K., Hanka, W., Wylegalla, K., Stavrakakis, G., Vafidis, A., Harjes, H. P. and Bohnhoff, M.: Lithospheric structure of the Aegean obtained from P and S receiver functions, J. Geophys. Res., 111, B12307, doi:.10.1029/2005JB003932, 2006.

Sodoudi, F., Yuan, X., Kind, R., Lebedev, S., Adam, J.M.-C., Kästle E. and Tilmann, F.: Seismic evidence for stratification in composition and anisotropic fabric within the thick lithosphere of Kalahari Craton. Geochem. Geophys. Geosyst.,14, 5393–5412, doi:10.1002/2013GC004955, 2013.

Sodoudi, F., Brüstle, A., Meier, T., Kind, R., Friederich, W. and EGELADOS working group: Receiver function images of the Hellenic subduction zone and comparison to microseismicity. Solid Earth, 6, 135-151, doi:10.5194/se-6-135-2015, 2015.

Şengör, A. M. C. and Kidd, W. S. F.: The post-collisional tectonics of the Turkish-Iranian Plateau and a comparison with Tibet: Tectonophysics, 55, 361-376, 1979.

Şengör, A.M.C., Özeren, S., Genç, T., Zor, E., 2003. East Anatolian high plateau as a mantle supported, north–south shortened domal structure. Geophys. Res. Lett. 30 (24), 8045. .http://dx.doi.org/10.1029/2003GL017858, 2003.

Tauzin, B., Debayle, E. and Wittlinger G.: Seismic evidence for global low-velocity layer within the Earth's upper mantle. Nature Geoscience 3, doi: 10.1038/NGEO969, 2010.

Taymaz, T., Jackson, J.A. and Westaway, R.: Earthquake Mechanisms in the Hellenic Trench near Crete. Geophys. J. Int., 102, 695-731, 1990.

Taymaz, T., Jackson, J.A. and McKenzie, D.: Active Tectonics of the North and Central Aegean Sea. Geophys. J. Int., 106, 433-490, 1991a.

Taymaz, T., Eyidogan, H. and Jackson, J.A. Source Parameters of large earthquakes in the East Anatolian Fault Zone (Turkey), Geophys. J. Int., 106, 537-550, 1991b.

Taymaz, T., Westaway, R. and Reilinger, R. (Guest Editors): Active Faulting and Crustal Deformation in the Eastern Mediterranean Region, Tectonophysics, Special Issue of 391, Issues 1-4, 375 pages, October 29, 2004. doi:10.1016/j.tecto.2004.07.005, 2004.

Vanacore E.A., Taymaz, T. and Saygin, E.: Moho structure of the Anatolian plate from receiver function analysis. Geophys. J. Int. 193(1),329-337, 2013.

Vinnik, L.P., Erduran, M., Oreshin, S.I., Kosarev, G.L., Kutlu, Y.A., Çakir, Ö., Kiselev, S.G.: Joint inversion of P- and S-receiver functions and dispersion curves of Rayleigh waves: The results for the Central Anatolian Plateau, Izvestiya, Physics of the Solid Earth, Volume 50, Issue 5, pp 622-631, 2014.

Wortel, M.J.R., and Spakman, W.: Subduction and slab detachment in the Mediterranean-Carpathian region: Science, v. 290, p. 1910–1917, doi: 10.1126/science .290 .5498.1910, 2000.

Yuan, X., Kind, R., Li, X. and Wang, R.: The S receiver functions; synthetics and data example. Geophys. J. Int. 165, 555–564 doi: 10.1111/j.1365-246X.2006.02885.x, 2006.

Zor, E., Sandvol, E., Gurbuz, C., Turkelli, N., Seber, D. and Barazangi, M.: The crustal structure of the East Anatolian plateau (Turkey) from receiver functions, Geophys. Res. Lett., 30(24), 8044, doi:.10.1029/2003GL018192, 2003.

Zor, E., Özalaybey, S. and Gürbüz, C.: The crustal structure of the eastern Marmara region, Turkey by teleseismic receiver functions, Geophys. J. Int., 167, 213–222, doi:10.1111/j.1365-246X.2006.03042.x, 2006.

Zor, E.: Tomographic evidence of slab detachment beneath eastern Turkey and the Caucasus, Geophys. J. Int., 175, 1273–1282, 2008.

Figure Captions

Figure 1: Tectonic map of the study area. The major plate boundary data are taken from Bird (2003). Subduction zones are pink, continental transform faults are red, continental rift boundaries are green, and spreading ridges boundaries are yellow. EAAC, NAF, EAF, DSF are the East Anatolian Accretionary Complex, North Anatolian Fault, East Anatolian Fault, Dead Sea Fault, respectively. X marks the Eratosthenes seamount.

Figure 2: a) Epicentral distribution of 1028 teleseismic events (Mw>5.5) with epicentral distances ranging from 60 to 85°, marked with red circles. b) Distribution of 195 analyzed broadband stations of the KOERI (triangles), GEOFON (circles), NOA-Net (squares) and HT-Net (diamonds) networks.

Figure 3: Stacks of all 11660 S-receiver functions as a function of the epicentral distance (binned in 0.5° distance windows). The traces are lined up along the theoretical arrival time of the SV phase. Data are deconvolved and filtered with a 8 s low-pass filter. Theoretical arrival times of several phases are marked.

Figure 4: Common conversion point (CCP) stacking results of synthetic S-receiver functions generated with the RAYSUM package (Frederiksen and Bostock, 2000) for different inclination angles of a high velocity zone (slab). The converters of the input models are depicted as black lines. The velocities used for the modeling are given in a). The locations of the converters as reconstructed by CCP stacking of the synthetic S-receiver function amplitudes are shown in red (positive) and blue (negative). As for the depth transformations, a 1D velocity model is used for calculating the conversion points, resulting in the offset between input and recovered anomalies for inclined discontinuities. g) The emergent angles (relative to the slab surface) of the Sp converted and transmitted waves are calculated in dependence of the back azimuth of the incident S-wave for the velocity contrast at the lower boundary of the slab. The results for the different considered inclination angles (dip) are shown in different colors. The range of back azimuths for which Sp converted energy is transmitted is getting smaller for increasing dipping angle.

Figure 5: Display of S-receiver functions along a north-south profile between 22 and 30°E (Aegean and western Anatolia). Topography is displayed on top of the figure. (a) CCP stack (depth–transformation). (b) Time-domain stack for same profile as in (a). A slowness of 6.4s/° are used for the move-out correction. The binning is determined by the location of piercing points at 200 km

depth. The numbers below the bottom y-axis show how many traces have contributed to each trace (c) Blue triangles are stations which contributed data to the profile. Red dots are locations of S-to-P piercing points at 200 km depth.

Figure 6: Same as Fig. 5 for a north-south profile between 30 and 39°E (central Anatolia). The width of this profile is too wide to see details of the subduction near Cyprus, see Fig. 8 for more details. No change in depth across the North Anatolian Fault is noticeable (NAF in (a)).

Figure 7: Same as Fig. 5 for a north-south profile between 38 and 47°E (eastern Anatolia). A flat Anatolian LAB is visible; no subducting LAB can be seen.

Figure 8: Same as Fig. 5 for an east-west profile between 34 and 37°N along southern Anatolia. The African LAB appears to deepening from near 100 km depth below the Aegean and western Anatolia to about 200 km depth at the western edge of Cyprus. Further to the east the LAB is strong and shallow. White circles projected on the migrated depth section of (a) represent the hypocenters of earthquakes between 1998 and 2014 (catalogue of International Seismological Center).

Figure 9: Same as Fig. 5 for an east-west profile between 37 and 41N along central Anatolia. LAB (white dashed line) and Moho (black dashed line) are marked in (a) and (b). Both phases are strong signals and slightly dipping from west to east. The Moho is in average in the west at about 25 km depth and in the east at about 40 km depth. The LAB depth deepens from about 80 km in the west to about 90 km in the east. Below the Aegean we see indications of the subducting African LAB.

Figure 10: Same as Fig. 5 for an east-west profile between 41 and 44N along northern Anatolia and the southern part of the Black Sea. The LAB appears very similar to the central Anatolian profile (Fig. 9).

Figure 11: Same S-receiver functions as in Fig. 6b for different filters: A) no filter, B) 2s low-pass filter, C) 4s low-pass filter and D) 8s low-pass filter. At shorter periods (A and B) the LAB (blue signal around 10 s) may consist of several smaller discontinuities. Only for the 6 and 8 s low-pass filters it appears as single discontinuity. In contrast, the Moho and the discontinuity at 410 km depth (red signals around 5 s and 45 s, respectively) remain as sharp single discontinuities at all periods, suggesting that this behavior is due to structure rather than to the higher noise levels at shorter periods.

Figures

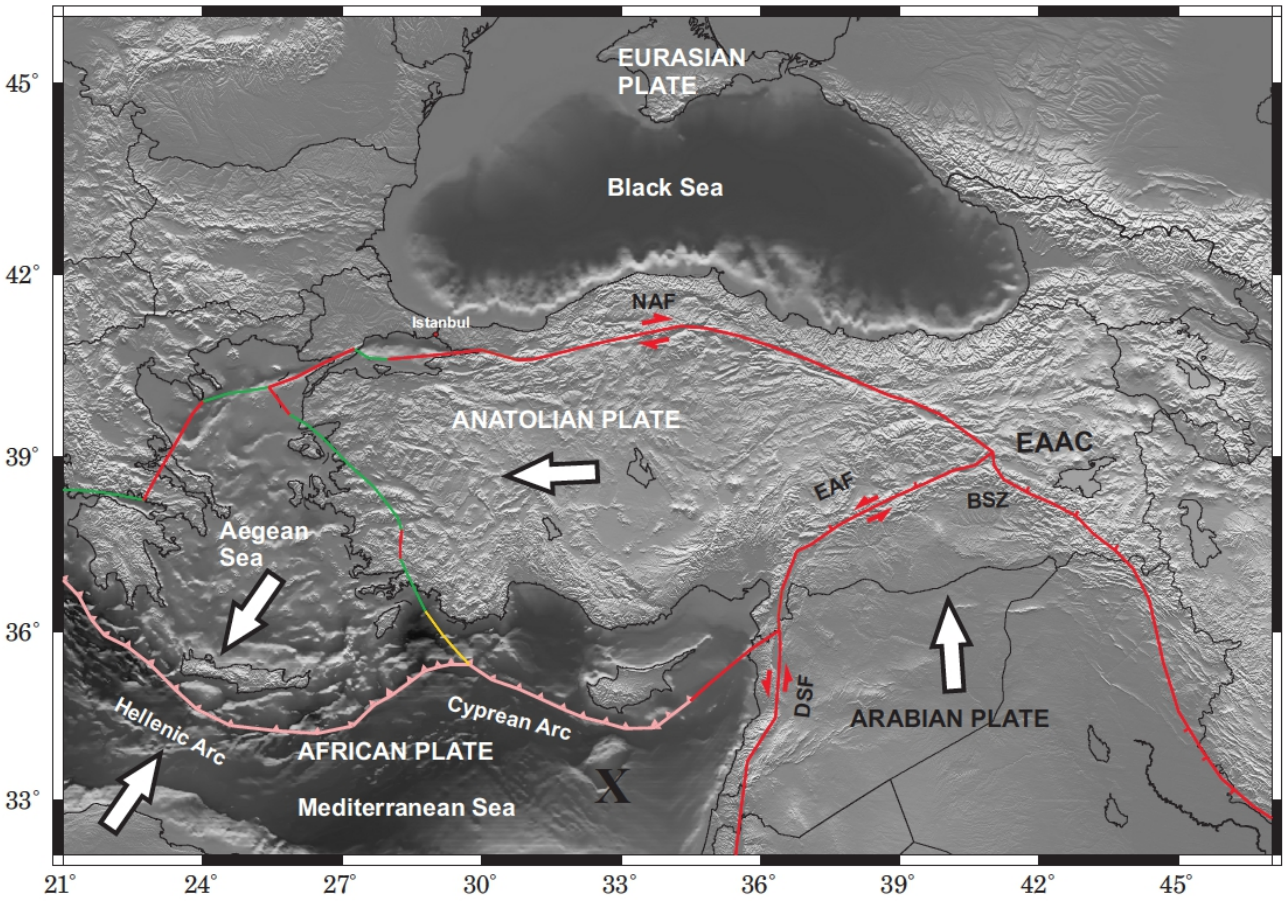

Figure 1: Tectonic map of the study area. The major plate boundary data are taken from Bird (2003). Subduction zones are pink, continental transform faults are red, continental rift boundaries are green, and spreading ridges boundaries are yellow. EAAC, NAF, EAF, DSF are the East Anatolian Accretionary Complex, North Anatolian Fault, East Anatolian Fault, Dead Sea Fault, respectively. X marks the Eratosthenes seamount.

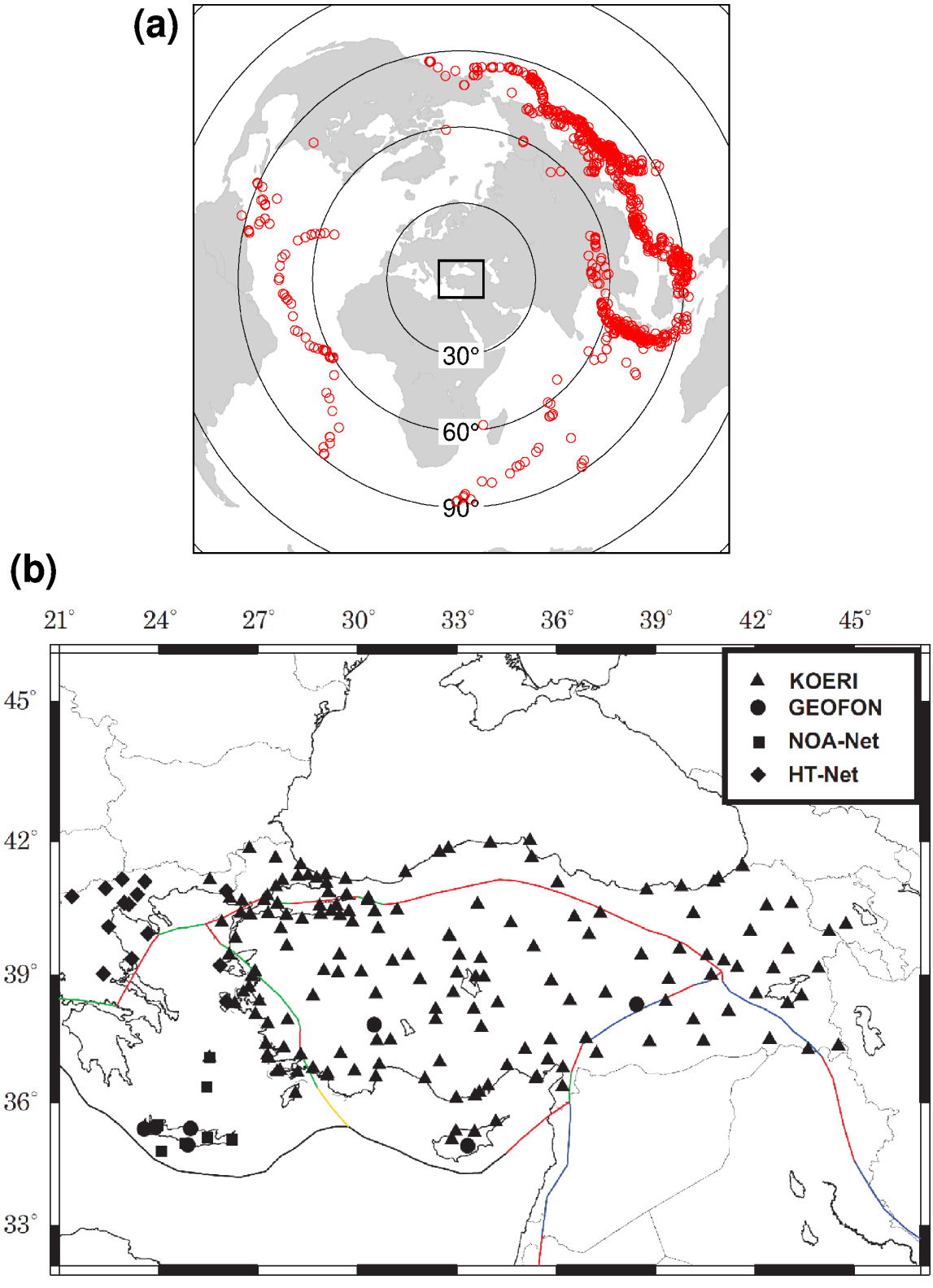

Figure 2: a) Epicentral distribution of 1028 teleseismic events (Mw>5.5) with epicentral distances ranging from 60 to 85°, marked with red circles. b) Distribution of 195 analyzed broadband stations of the KOERI (triangles), GEOFON (circles), NOA-Net (squares) and HT-Net (diamonds) networks.

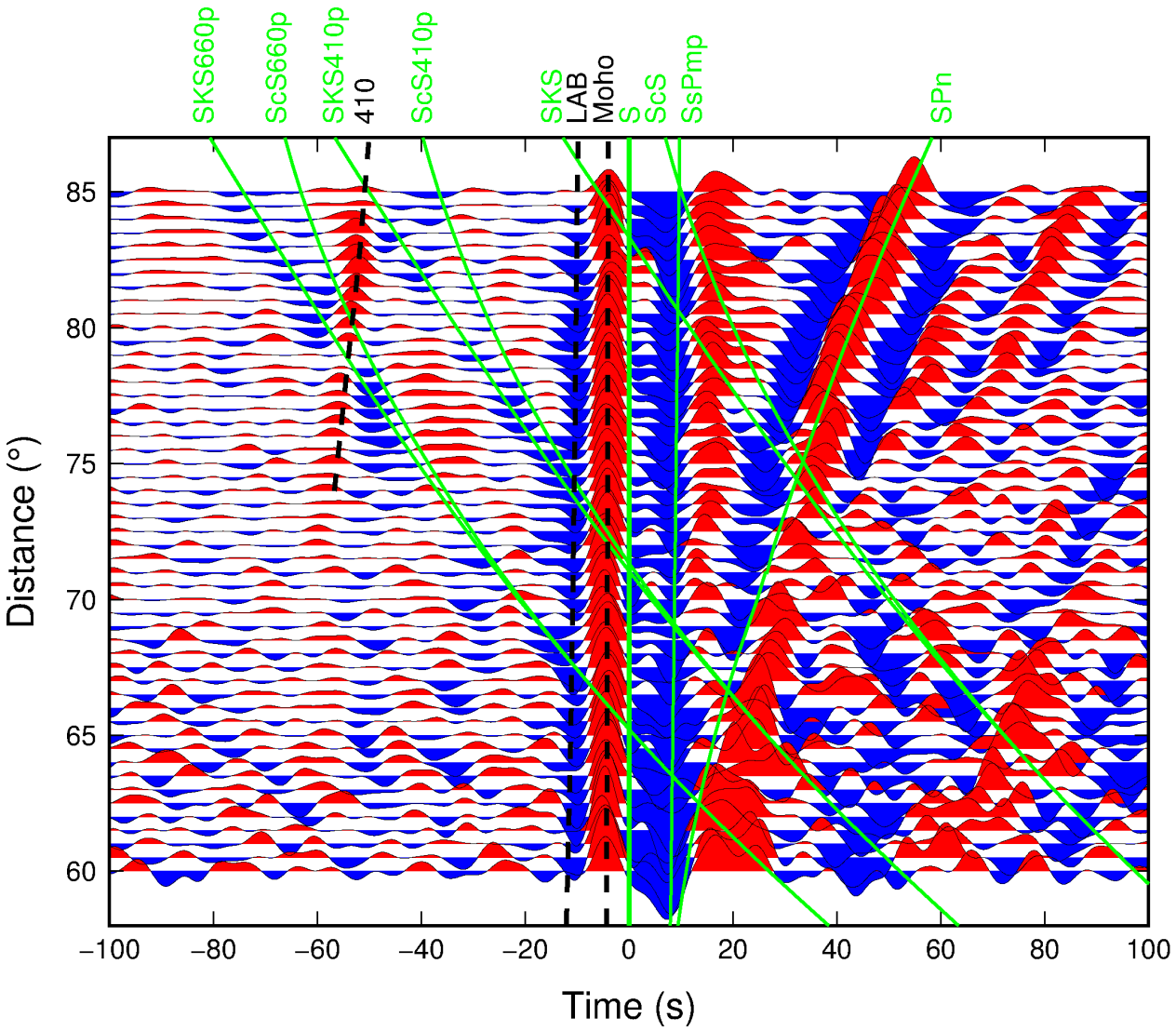

Figure 3: Stacks of all 11660 S-receiver functions as a function of the epicentral distance (binned in 0.5° distance windows). The traces are lined up along the theoretical arrival time of the SV phase. Data are deconvolved and filtered with a 8 s low-pass filter. Theoretical arrival times of several phases are marked.

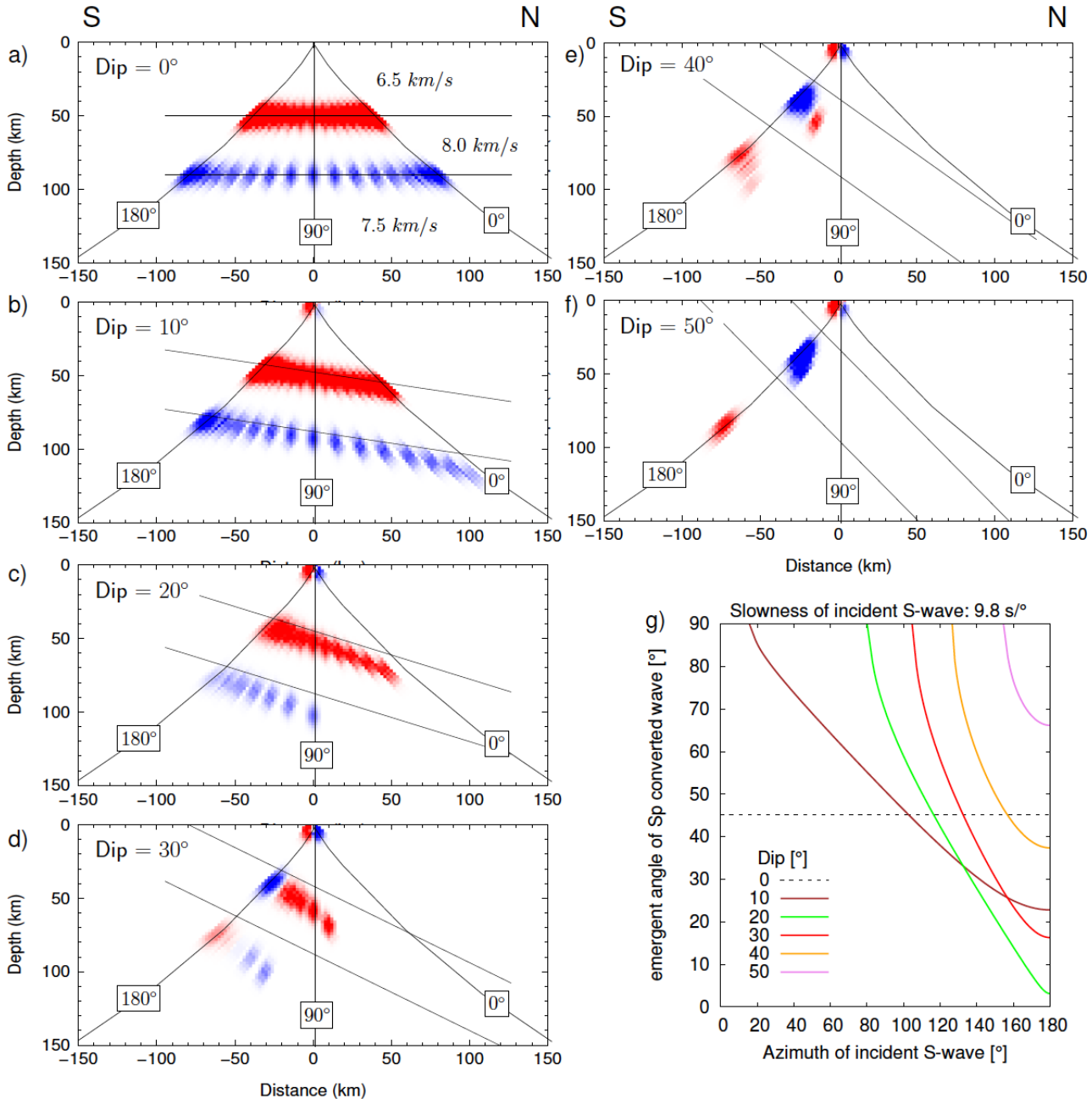

Figure 4: Common conversion point (CCP) stacking results of synthetic S-receiver functions generated with the RAYSUM package (Frederiksen and Bostock, 2000) for different inclination angles of a high velocity zone (slab). The converters of the input models are depicted as black lines. The velocities used for the modeling are given in a). The locations of the converters as reconstructed by CCP stacking of the synthetic S-receiver function amplitudes are shown in red (positive) and blue (negative). As for the depth transformations, a 1D velocity model is used for calculating the conversion points, resulting in the offset between input and recovered anomalies for inclined discontinuities. g) The emergent angles (relative to the slab surface) of the Sp converted and transmitted waves are calculated in dependence of the back azimuth of the incident S-wave for the velocity contrast at the lower boundary of the slab. The results for the different considered inclination angles (dip) are shown in different colors. The range of back azimuths for which Sp converted energy is transmitted is getting smaller for increasing dipping angle.

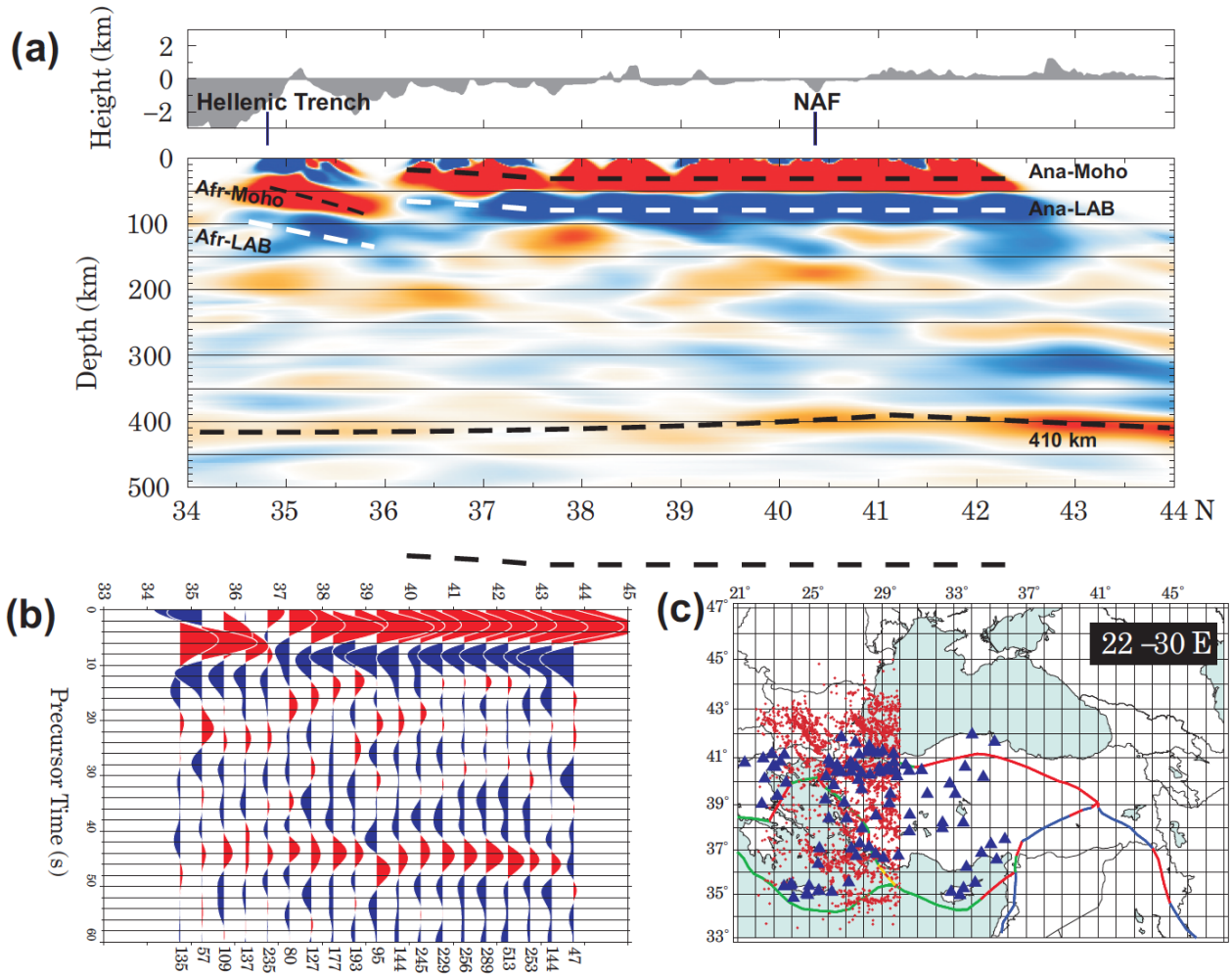

Figure 5: Display of S-receiver functions along a north-south profile between 22 and 30°E (Aegean and western Anatolia). Topography is displayed on top of the figure. (a) CCP stack (depth–transformation). (b) Time-domain stack for same profile as in (a). A slowness of 6.4s/° are used for the move-out correction. The binning is determined by the location of piercing points at 200 km depth. The numbers below the bottom y-axis show how many traces have contributed to each trace (c) Blue triangles are stations which contributed data to the profile. Red dots are locations of S-to-P piercing points at 200 km depth.

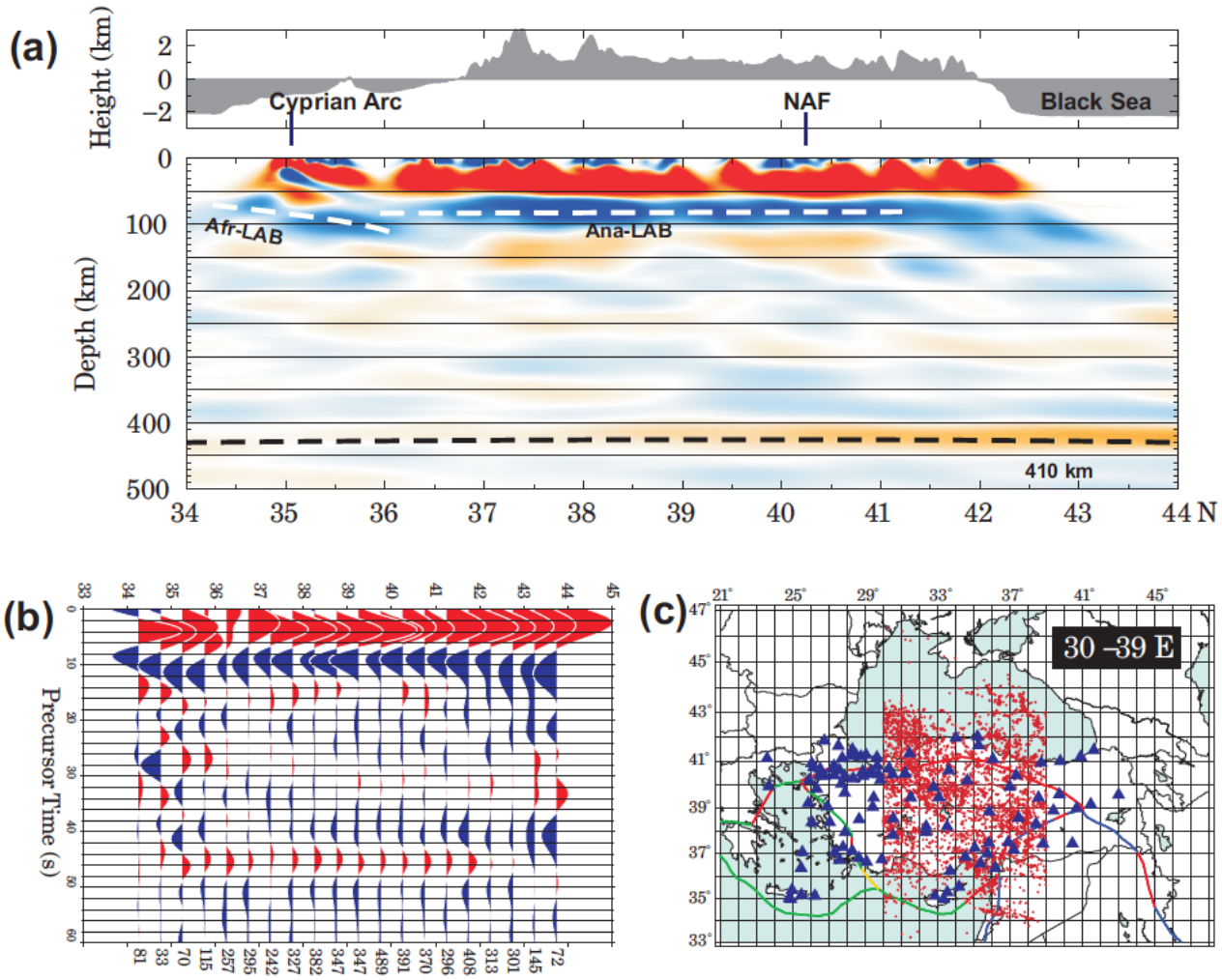

Figure 6: Same as Fig. 5 for a north-south profile between 30 and 39°E (central Anatolia). The width of this profile is too wide to see details of the subduction near Cyprus, see Fig. 8 for more details. No change in depth across the North Anatolian Fault is noticeable (NAF in (a)).

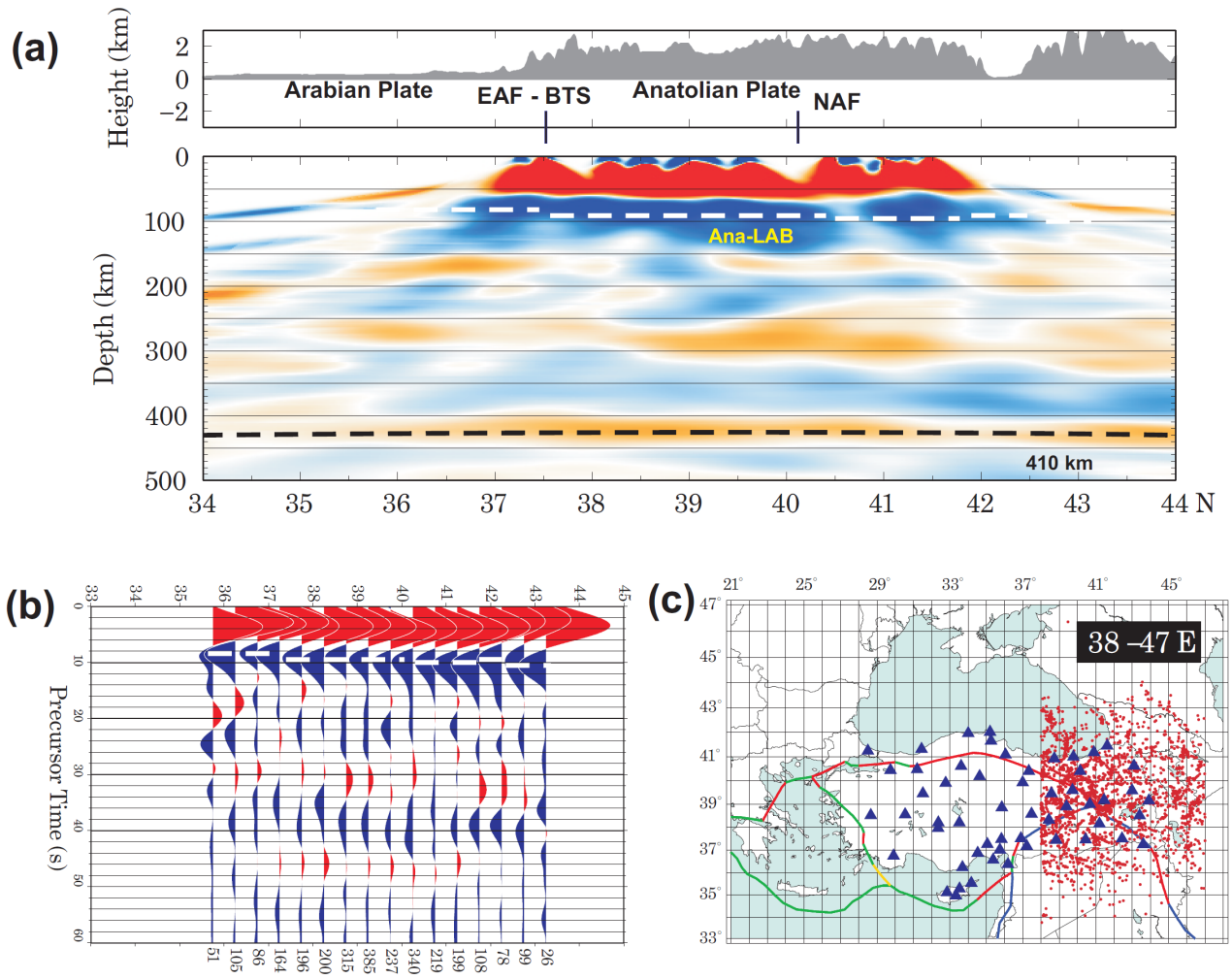

Figure 7: Same as Fig. 5 for a north-south profile between 38 and 47°E (eastern Anatolia). A flat Anatolian LAB is visible; no subducting LAB can be seen.

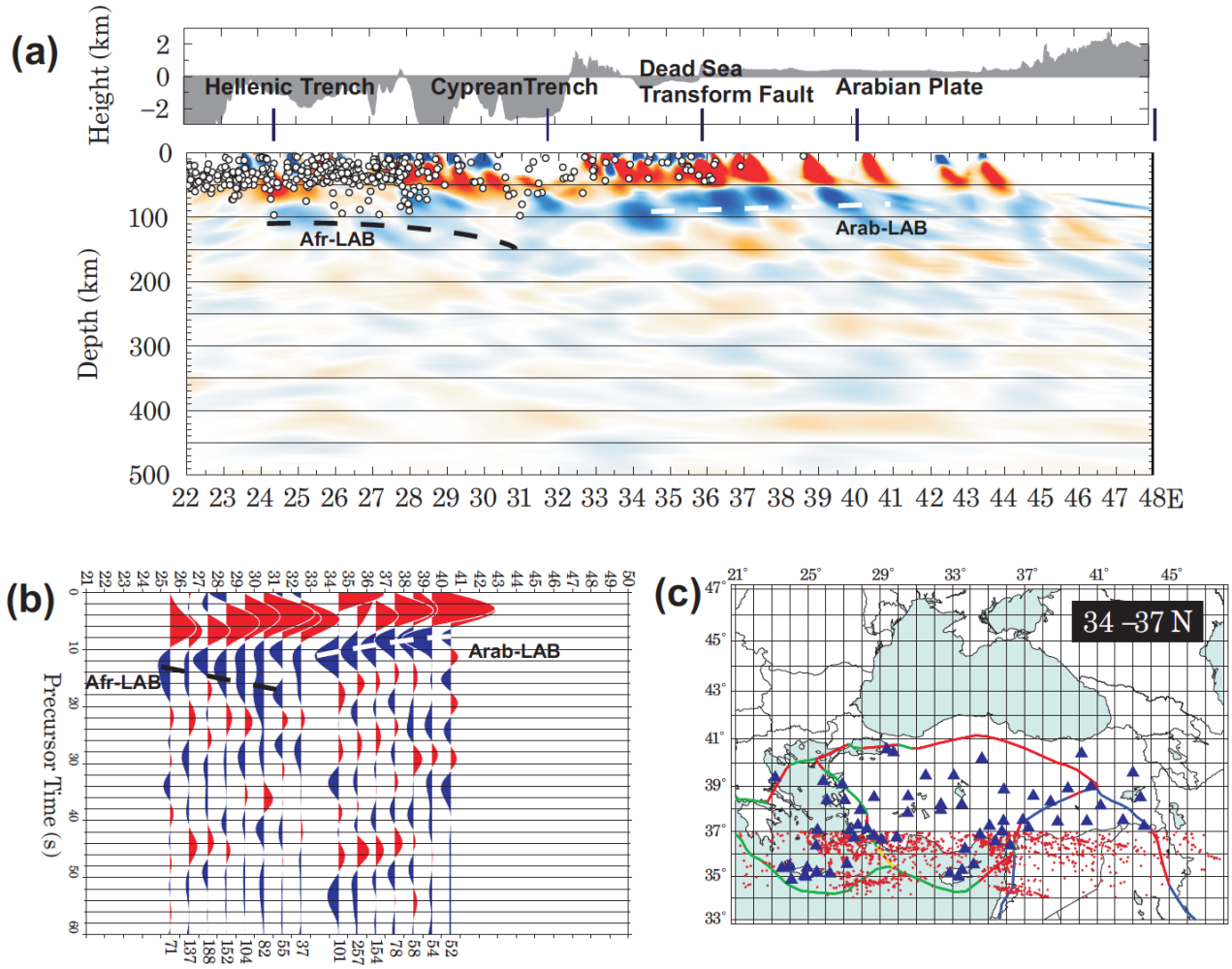

Figure 8: Same as Fig. 5 for an east-west profile between 34 and 37°N along southern Anatolia. The African LAB appears to deepening from near 100 km depth below the Aegean and western Anatolia to about 200 km depth at the western edge of Cyprus. Further to the east the LAB is strong and shallow. White circles projected on the migrated depth section of (a) represent the hypocenters of earthquakes between 1998 and 2014 (catalogue of International Seismological Center).

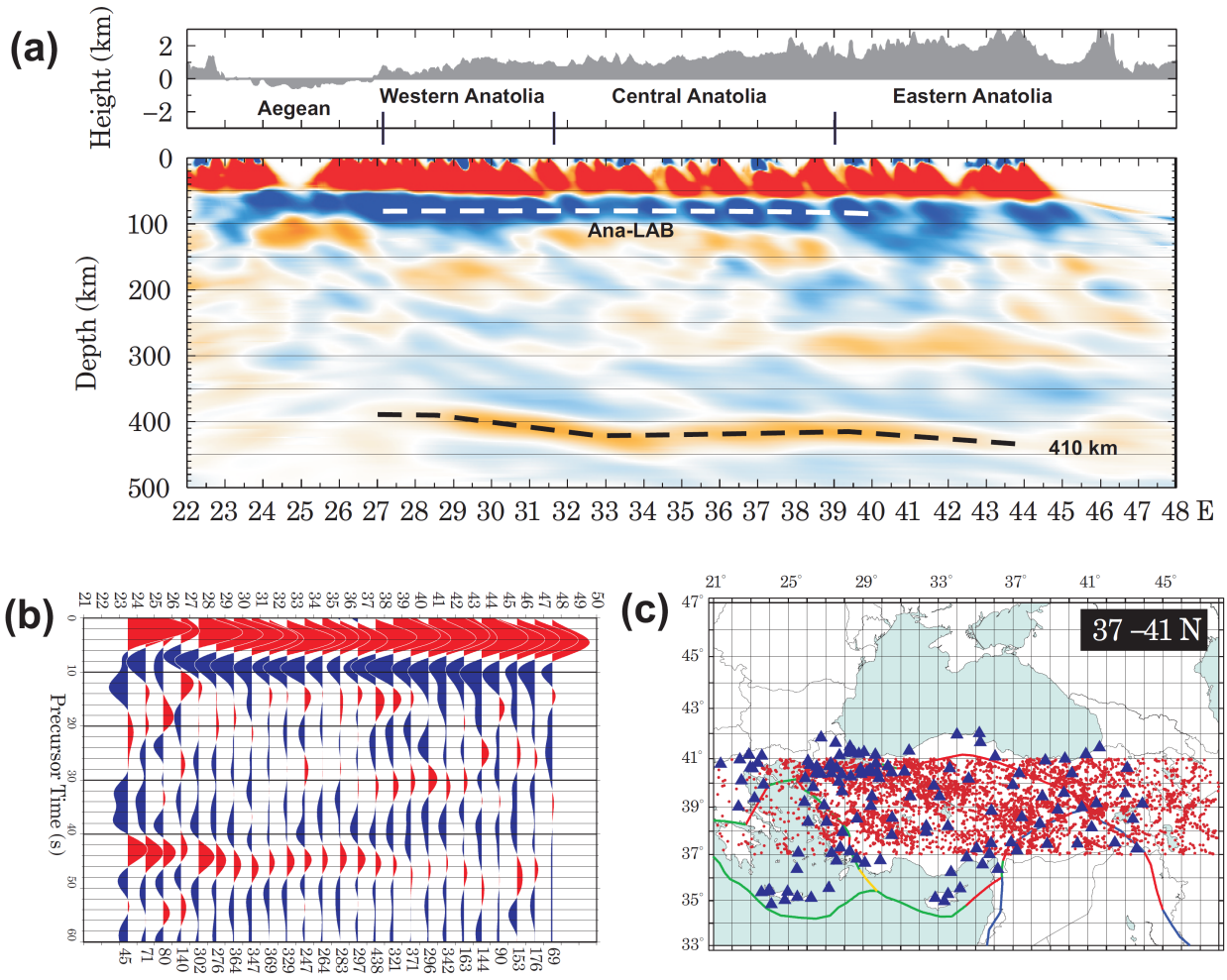

Figure 9: Same as Fig. 5 for an east-west profile between 37 and 41N along central Anatolia. LAB (white dashed line) and Moho (black dashed line) are marked in (a) and (b). Both phases are strong signals and slightly dipping from west to east. The Moho is in average in the west at about 25 km depth and in the east at about 40 km depth. The LAB depth deepens from about 80 km in the west to about 90 km in the east. Below the Aegean we see indications of the subducting African LAB.

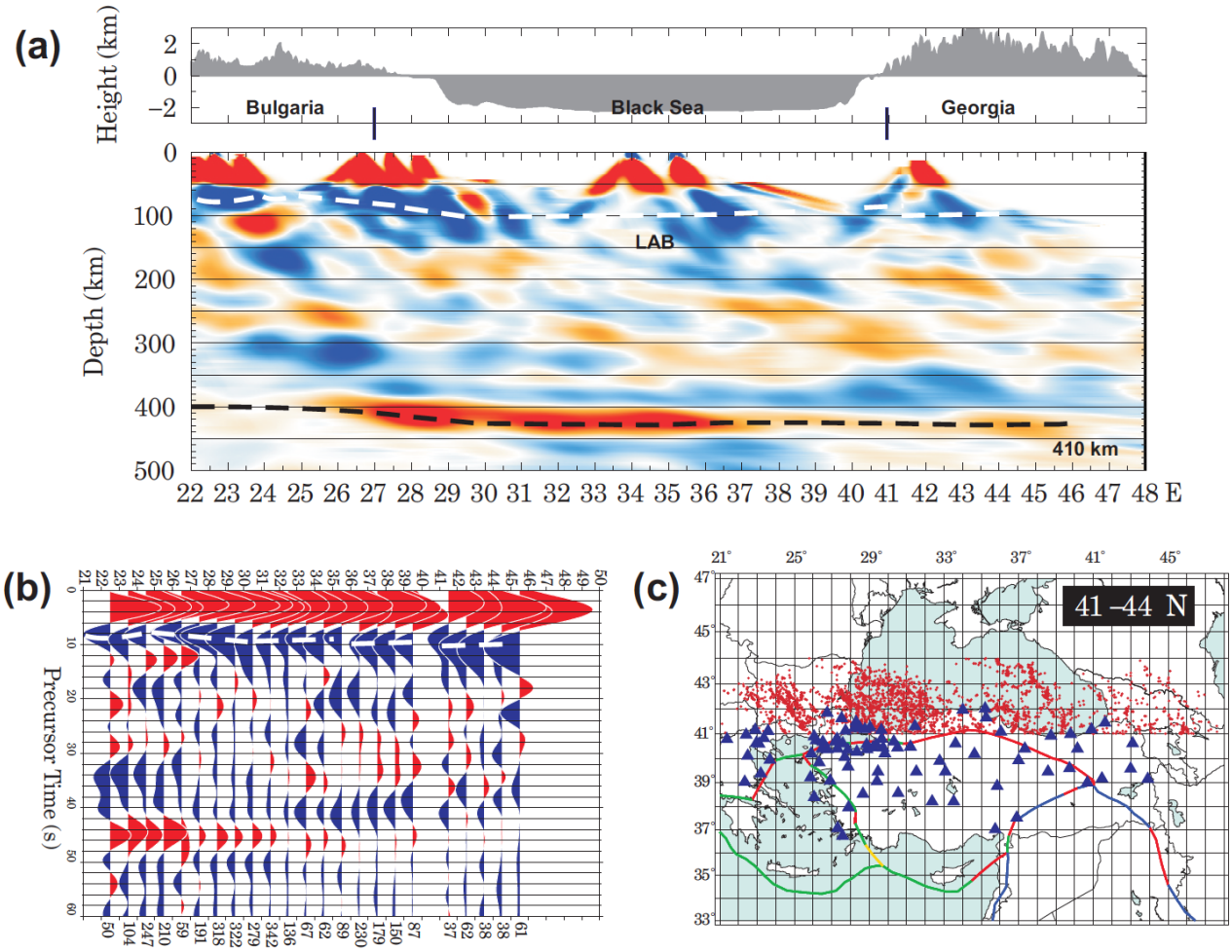

Figure 10: Same as Fig. 5 for an east-west profile between 41 and 44N along northern Anatolia and the southern part of the Black Sea. The LAB appears very similar to the central Anatolian profile (Fig. 9).

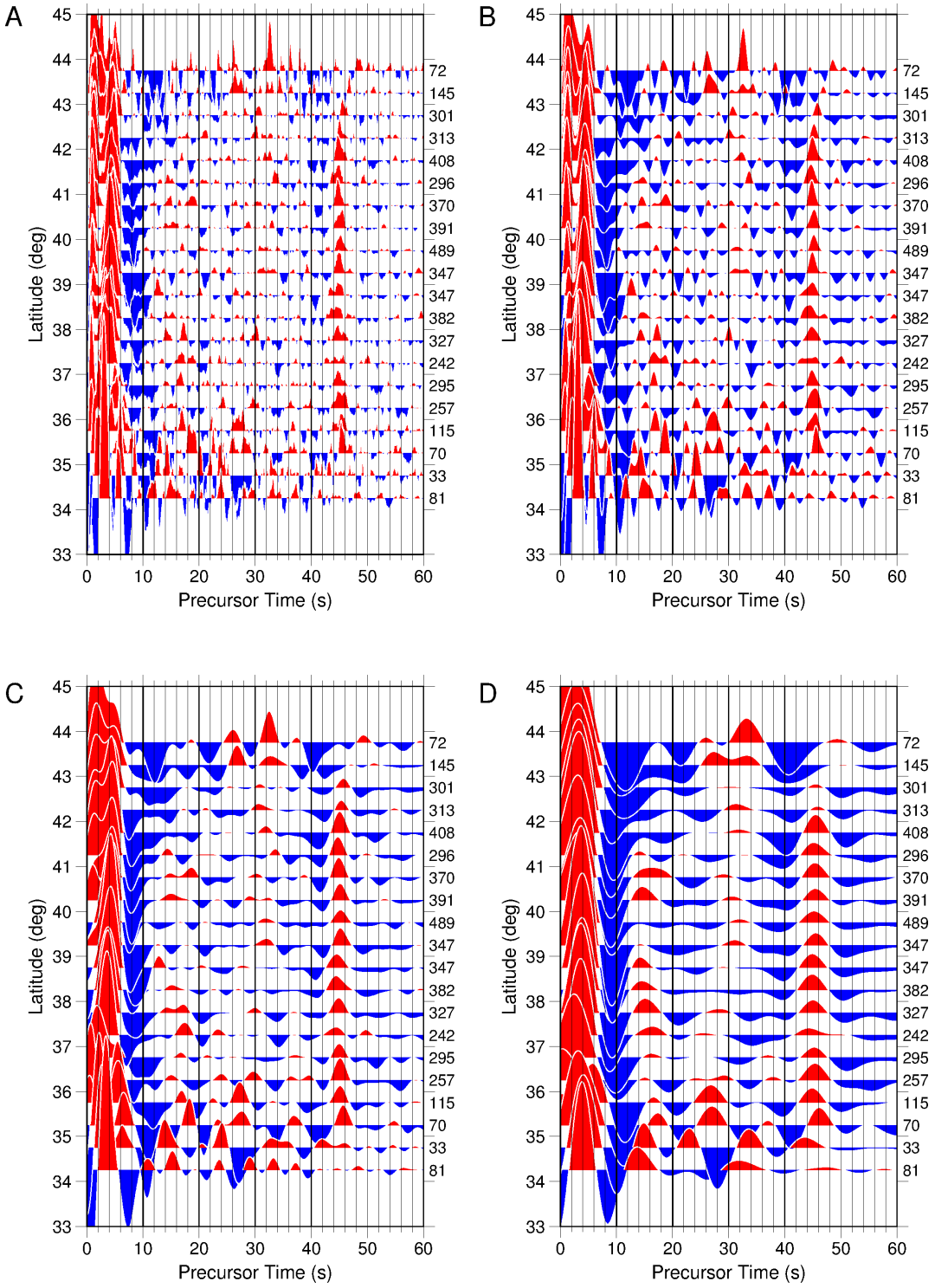

Figure 11: Same S-receiver functions as in Fig. 6b for different filters: A) no filter, B) 2s low-pass filter, C) 4s low-pass filter and D) 8s low-pass filter. At shorter periods (A and B) the LAB (blue signal around 10 s) may consist of several smaller discontinuities. Only for the 6 and 8 s low-pass filters it appears as single discontinuity. In contrast, the Moho and the discontinuity at 410 km depth (red signals around 5 s and 45 s, respectively) remain as sharp single discontinuities at all periods, suggesting that this behavior is due to structure rather than to the higher noise levels at shorter periods.